PAPER • OPEN ACCESS

A hierarchical supervisory wind power plant controller

View the article online for updates and enhancements.

A hierarchical supervisory wind power plant controller

Karl Merz*, Valentin Chabaud, Paula B. Garcia-Rosa and Konstanze Kölle

SINTEF Energy Research, Sem Sælands vei 11, 7034, Trondheim, Norway

E-mail: `Karl.Merz@sintef.no`

Abstract.   The operation of future wind power plants (WPPs) will rely on maximizing overall profit rather than power production. Factors like current electricity price, grid code compliance, and maintenance costs will affect operational decision. Therefore, it is expected that plant control strategies will trade different control objectives while respecting the industrial practice, where the different levels in the hierarchy may be provided by different equipment vendors. This work proposes a plant controller that aims to track an operator power command at the WPP level and to reject low-frequency loading due to turbulent winds at individual turbines. The plant control respects the hierarchy in which the turbine-level controller takes precedence, interacting only via power set-point commands to each turbine. The control algorithm is based on parallel control loops along with look-up tables and gain scheduling, and its simplicity and effectiveness make it well-suited for industrial applications. Preliminary simulation results with a 32-turbine WPP indicate that there is a significant synergy effect by coordinating operation of the turbines in a plant. Structural loads can be reduced on certain turbines without excessively burdening the others, while an accurate plant-wide power tracking is still provided.

1. Introduction

Operating a wind power plant (WPP) in the future will aim to maximise the revenue rather than maximising the power production. Future WPPs are expected to participate in volatile electricity markets and to provide ancillary services. Beyond the amount of the produced power, other factors such as the current electricity price and operation and maintenance costs will affect operational decision. The reduction of structural loading and actuator wear will become more important in this context.

Tracking an external power command provides degrees of freedom to consider additional objectives when dispatching the power between the turbines. The common industrial practice is to use a static power dispatch, either by equally distributing the power reference among the turbines or by manually choosing the distribution factors for curtailment. Static dispatch has the disadvantage that a turbine may not be able to meet the requested power (reserve) due to unconsidered aerodynamic interactions inside the WPP. The proportional dispatch overcomes these shortcomings by dynamically defining the power set-points based on the estimated available power at each turbine [1].

Achieving an optimised dispatch for multi-objective WPP control has been targeted with e.g. model predictive control and other optimization-based approaches [2–5]. The general applicability of a model-predictive optimization approach into the industrial practice was

demonstrated by numerical simulation studies with a large scale wind turbine in [5]. In this case, a linear model was employed to estimate the turbines' available power. However, the high computational cost of optimization-based control strategies is often hindering industrial implementation. A simple controller, that trades distinct control objectives while respecting the existing industrial control hierarchy practice, can also be beneficial to serve as a baseline for comparison against more advanced control strategies.

When a wind power plant is operating with a reserve, whether curtailed or overplanted, it should be able to provide ancillary services by adapting the power production to actual needs. In this case, there will be a margin of flexibility in the operation of each wind turbine, which can be used beneficially, for instance, to reject fluctuating loads. Thus, the control objective pursued in this study is to track the operator power command at the wind power plant level while rejecting low-frequency loading due to turbulent winds at individual turbines. Drawing inspiration from [6], the control architecture consists of parallel control loops performing each function, i.e. active load control and power tracking, along with some look-up tables and gain scheduling. The proposed control is simple and accessible, and then, it can also be useful as a baseline controller.

Low-frequency shaft torque and thrust force are common variables in control-oriented models [3, 7]. The damage equivalent load (DEL), which is more relevant for the fatigue, can only be calculated from the load history. To provide it as a measure for real-time control decisions, the DEL for similar inflow and operational conditions can be computed online [8] or extracted from pre-calculated databases. High-fidelity simulations have been used to create look-up tables [4, 9–12] or to identify neural-network models [13, 14]. However, this study assumes that the current loading or component wear rates are available for relevant components, focusing on the design of the plant controller.

Simulation results illustrate the performance of the plant controller when it is applied to the TotalControl Reference Wind Power Plant [15]. In this case, the WPP is under curtailment, i.e. the operator has provided a power command that lies under the maximum possible production, given the present wind conditions. It is found that there is a meaningful synergy in coordinating the control of wind turbines in a large power plant: loads can be reduced on turbines that need it the most without excessively burdening the other turbines, while still providing accurate plant-wide power tracking.

2. Overview of the wind power plant model

Figure 1 shows a high-level block diagram of a wind power plant and its surroundings, including the interface variables between the wind plant and the plant control. In the block diagram,

- the wind plant consists of the wind turbines and their individual controllers, local wakes and their corresponding induced velocity, collection grid, and electrical transmission system to the point of common coupling (PCC) with the main electric grid;

- the atmosphere consists of the surrounding flow that mixes with the turbine wakes and the ambient, else undisturbed, turbulent wind;

- the electric grid here refers to the regional grid to which the wind plant is connected; and

- the plant control consists of a hierarchical control architecture that coordinates the control of the wind turbines.

The wind plant sends the induced velocity ($\mathbf{V}_i$) caused by the vortical wake of each turbine to the atmosphere block and receives in return the effective wind velocity ($\mathbf{V}$) approaching each wind turbine. The wind plant also sends a three-phase electrical current waveform ($\boldsymbol{i}^{\theta}_{\mathrm{PCC}}$) to the PCC bus, while the grid provides the bus voltage ($\boldsymbol{v}^{\theta}_{\mathrm{PCC}}$). The electrical variables are in the d-q frame, which is labelled with a superscript θ here. The d-q frame maps three-phase time-varying
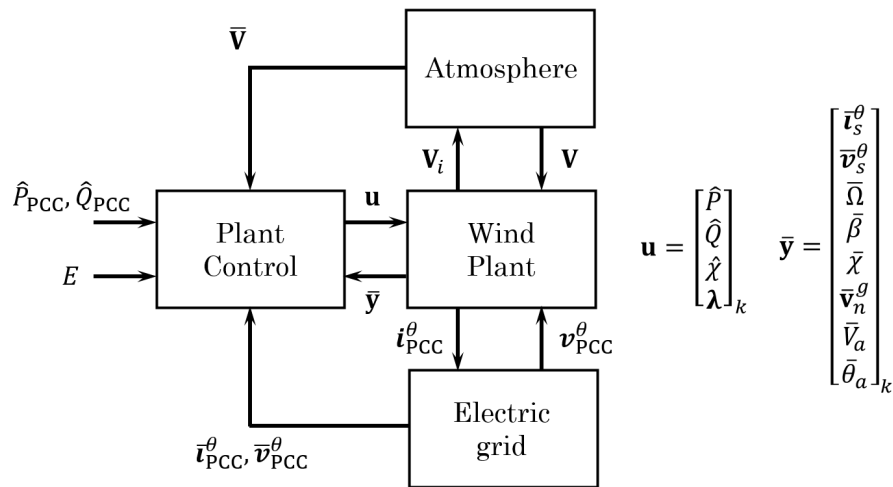
Figure 1. A high-level block diagram of a wind power plant and its surroundings, showing the interface variables with the plant control ($\mathbf{u}$ and $\bar{\mathbf{y}}$).

currents and voltages to 2-D space vectors rotating at an imposed speed, which simplifies the calculations.

From the wind plant block, the plant controller receives the current and voltage waveforms ($\bar{\boldsymbol{\imath}}_s^\theta$, $\bar{\boldsymbol{v}}_s^\theta$) at the transformer high-voltage terminals, the rotor speed ($\overline{\Omega}$), the collective blade pitch ($\overline{\beta}$), the nacelle yaw angle ($\overline{\chi}$), the absolute nacelle velocity ($\overline{\mathbf{v}}_n^g$), which is measured by an inertial measurement unit, the anemometer wind speed ($\overline{V}_a$), and the anemometer wind angle ($\overline{\theta}_a$). Then, it provides the set-point commands of active and reactive power ($\hat{P}$, $\hat{Q}$) and yaw angle ($\hat{\chi}$) to each wind turbine controller. In addition to these commands, the variable $\boldsymbol{\lambda}$ shown in Fig. 1 may contain flags to set the turbines' operating mode, if the turbine controller allows for this. Notice that reactive power control and an electric grid model will not be considered in this work. The plant control algorithm will be described in Section 3.

2.1. Wind plant model

A wind farm with N identical wind turbines is considered. Figure 2 illustrates the main components of the wind plant model, where all variables in the turbine components and controller are associated to the k-th turbine of the plant: $\hat{P}_{ck}$ is the power command, $\hat{\beta}_k$ is the collective pitch angle, $\bar{M}_k$ is the blade root moments, q_k and $\dot{q}_k$ are structural positions and velocities, F_{ak} is the blade force, $T_{\beta k}$ is the blade pitch torque, T_{gk} is the generator torque, ω_{gk} is the generator electrical speed, and $(i_{gk}^\theta)_q$ is the current command. v_o^θ and i_o^θ are, respectively, voltage and current at the offshore substation.

Here, the turbine components are modelled as in [16, Chapter 5.3]. Assuming normal operating conditions, the aerodynamic model is based on the blade element momentum (BEM) method, which provides a sufficiently accurate estimate of the flow conditions at the rotorplane. The structural model is formulated using finite beam elements under the assumption of lateral structure deformation as a third order polynomial between predefined nodal locations. The model represents the tower, nacelle, driveshaft/hub, and blades. The pitch actuator is represented by a second order transfer function reproducing the dominant dynamics up to a frequency of several Hz. The electrical model of each wind turbine consists of a permanent magnet synchronous generator with full power converter and a transformer that steps up the generated voltage to the appropriate voltage for the collection grid, that is 66 kV here. For more
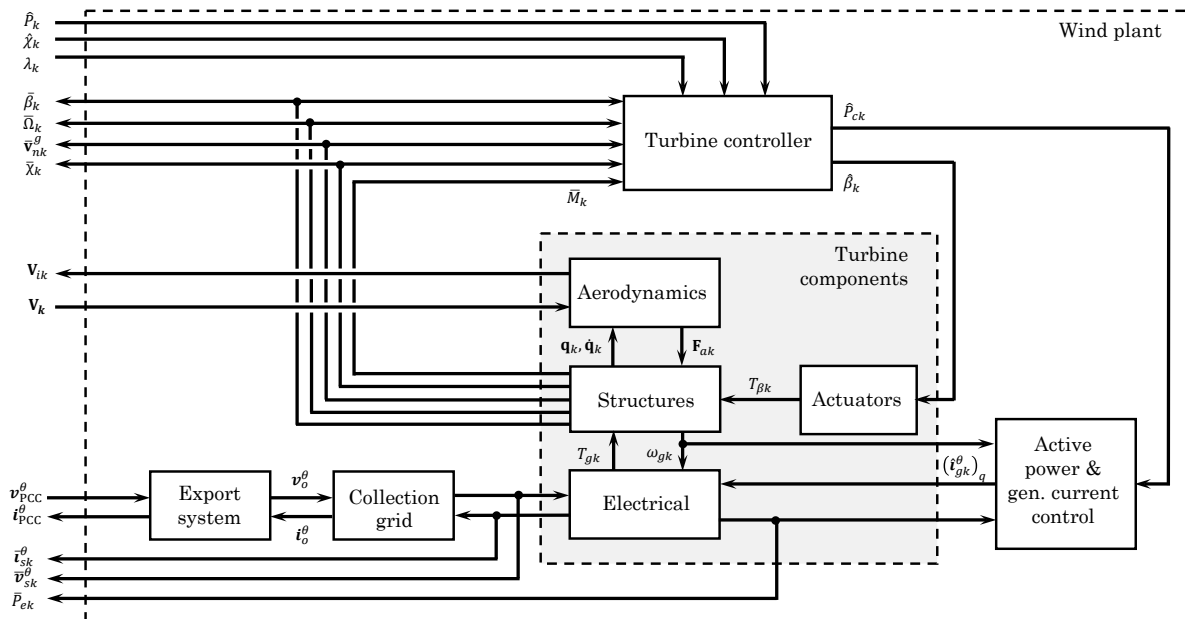
Figure 2. Block diagram with main components of the wind plant model.

details on the mathematical models, refer to [16, Chapter 5.3] and the references therein.

Each wind turbine controller in Fig. 2 implements the commanded set-points by the plant controller, to the extent possible, through coordinated control of its generator (via a power converter) and blade pitch. It also provides other necessary functions like keeping the rotor speed within limits and communicating status back to the plant supervisory controller. The control architecture adopted here is based on complete industrial-type wind turbine controllers, as described in [17].

The collection grid comprises the electrical cables connecting the turbines to an offshore substation. Then, the mathematical model consists of the dynamic equations of the π-equivalent circuit model, that represents the model of a medium-length transmission line, for each one of the cables connecting the turbines and the substation. The export system consists of electrical offshore and onshore substations with transformers, cables, and reactive compensation by the onshore substation.

2.2. Atmosphere model

The current framework is essentially based on analytical state-space modeling of plant dynamics, requiring explicit relationships between states, their derivatives, inputs and outputs. When it comes to farm flow, particularly complex physics are involved, typically only captured by costly computational fluid dynamics (CFD) simulations. While widely used, reduced-order models computing the wind velocity deficit and added wake turbulence intensity are steady state values, hence not appropriate for dynamic simulations. Other models such as the dynamic wake meandering model are challenging to translate to a state-space representation of reduced complexity, as it implies a discretization in space with states at each grid point over the whole farm area with non-explicit (algebraic) mathematical relations. Modeling the atmosphere block directly from physics appears then inherently uncertain compared to its wind plant, grid or farm controller counterparts. Shifting paradigm, it may be argued that the most accurate information about farm flow is provided by the turbines themselves, as observers of their environment through
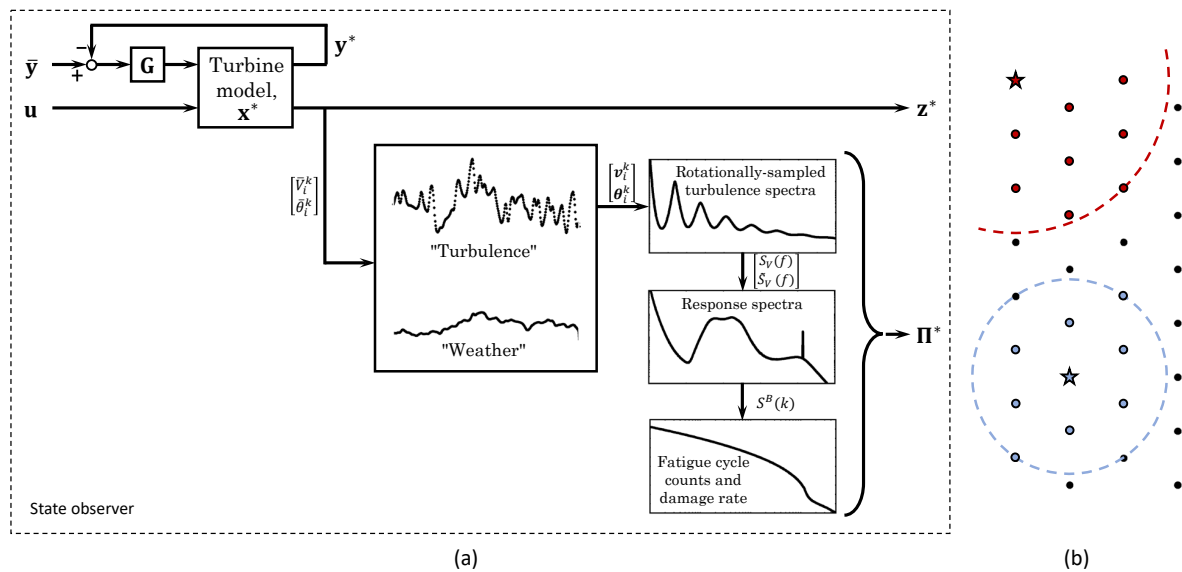
Figure 3. (a) The architecture of a state observer, showing the embedded wind turbine model, a module that distinguishes local turbulence from broader weather patterns, and an analytical spectral model that estimates the severity of loading and fatigue; (b) Examples of two turbine clusters for estimation of cluster wind speed and direction at the starred turbines.

their measurable response.

This approach is described in detail in [8] and only a brief summary is given here. The concept consists of dividing the flow into a *Turbulence* and a *Weather* part, as illustrated in Fig. 3.a. The *Turbulence* part represents high-frequency fluctuations linked to relatively small vortices and hence turbine-specific (no correlation between turbines). It is responsible for aeroelastic vibrations and corresponding loads, modeled via their spectral representation. The *Weather* part represents large, low-frequency coherent and/or transient flow structures. It is responsible for farm-wide power fluctuations and is modeled explicitly in a Bayesian framework by identifying correlated flow patterns in clusters of turbines, thereafter referred to as the *cluster wind speed* μ_v. Cluster wind speed observations of the *Weather* part are used to fit a parametric spectral representation of the *Turbulence* part, that is in turn used to derive loads and fatigue damage (Fig. 3.a). For each turbine, a cluster is defined here as the wind turbine plus its nearest eight neighbors where the turbines are arranged in an array of approximately uniform spacing, as illustrated in Fig. 3.b.

3. Hierarchical control

In this work, the primary objective of the wind plant controller is to deliver the demanded active power $\hat{P}_{\text{PCC}}$ at the PCC with the electric grid. The actual power must accurately track the set-point on a timescale of seconds, such that the wind plant provides primary frequency support to the grid. The secondary objective is to reduce the levels of loading and fatigue in the turbines. However, the secondary objective is considered only after the primary objective is satisfied.

3.1. Control architecture

Drawing inspiration from [6], the control architecture is based on parallel control loops: one loop provides the "ideal" active load control for each turbine, and the other provides a correction to
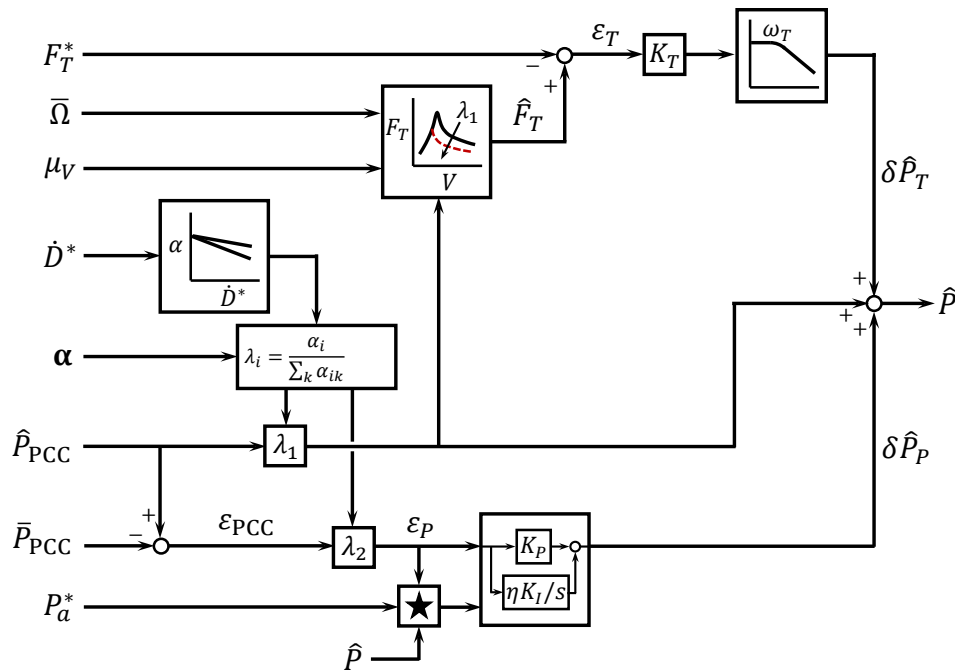
Figure 4. Architecture of the wind plant control law. The starred block provides anti-windup features.
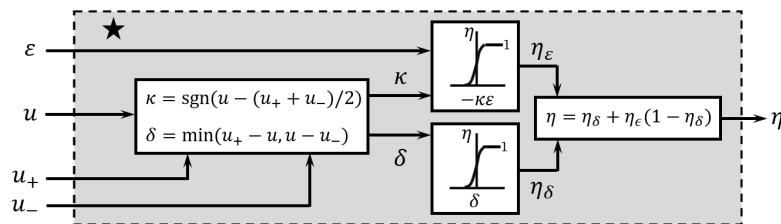

Figure 5. Anti-windup strategy.

the power set-point. This ensures that the overall plant power equals that commanded by the operator, to the extent that wind conditions allow. Then, the problem is not how to *dispatch power set-points*, but to *dispatch power corrections* to the turbines in the plant. There is little correlation in turbulent wind speed fluctuations from one turbine to the next, and when averaged over a large wind plant, the corrections will tend to be small. In this way, the active load control function can be considered independently of the plant power command tracking function.

Figure 4 shows the proposed control law, where the turbine's nominal share of the plant power command $\hat{P}_{\text{PCC}}$ is provided as a feed-through pathway without control dynamics, except those provided by the filtering of input signals. Power tracking and thrust compensation are provided by the two pathways, $\delta\hat{P}_P$ and $\delta\hat{P}_T$, as corrections to the nominal output. The pathways have different response characteristics: the power-tracking branch is a proportional-integral (PI) controller, while the thrust-compensation branch is a proportional controller with a low-pass filter. The control law is repeated for each turbine in the WPP, and in such a way, the integration of the error that ensures tracking in the plant power (ε_{PCC}) is done separately for each turbine. Therefore, gain-scheduling via λ can be done *inside* the integrator, as is proper; and saturation can be customized to fit the operating conditions of each turbine.

The two main pathways calculate $\delta\hat{P}_P$ and $\delta\hat{P}_T$ informed by estimates of the cluster wind speed μ_V, the component wear rate $\dot{D}^*$, which can be estimated by the spectral model as in Fig.3.a, the available power P_a^* based on the current wind conditions, and the rotor thrust F_T^*. Here, P_a^* and F_T^* are respectively estimated as

$$P_a^* \;=\; \frac{\rho A}{2} C_p^{"} (V^*)^3 \,, \tag{1}$$

$$F_T^* \;=\; \frac{\rho A}{2} C_T^{"} (V^*)^2 \,, \tag{2}$$

where ρ is the air density, A is the rotor swept area, R is the blade radius, V^* is the estimated wind speed, $C_P^{"}$ is the maximum power coefficient of the turbine and $C_T^{"}$ is the thrust coefficient. Here, we assume that all variables denoted with '*' are known. For practical application studies, an observer that provides state estimates at the wind turbines should be implemented.

3.1.1. Scheduling as a function of damage rate   The nominal power in the feed-through pathway and the gains on the power-tracking controller are scheduled as a function of the damage rate $\dot{D}^*$, as illustrated in Fig. 4. The scheduling is determined by the functions $\alpha_1(\dot{D}^*)$ and $\alpha_2(\dot{D}^*)$. Here, a simple relationship is considered,

$$\alpha_1 = 1 - 0.1\dot{D}^* \quad \text{and} \quad \alpha_2 = 1 - \dot{D}^* \,, \tag{3}$$

where a generic normalized damage rate takes a value between 0 (low damage) and 1 (high damage). As the damage rate increases from 0 to 1, the nominal share of the turbine's power, for determining the target thrust, drops from 1 to 0.9, while the power-tracking gain factor drops from 1 to 0. In this way, turbines with the highest damage metric do not contribute to balancing plant power. The jth turbine in the WPP gets its share of the power set-point by weighting according to

$$\lambda_{1,j} = \frac{\alpha_{1,j}}{\sum_{k=1}^{N} \alpha_{1,k}} \,, \tag{4}$$

where N is the total number of turbines in the plant. $\lambda_{2,j}$ is calculated in a similar way as (4).

3.1.2. Lookup table The target thrust $\hat{F}_T$ is set according to the wind turbine's typical $C_T(\text{TSR}, \beta)$ table, where $\text{TSR} = R\Omega/V_\infty$ is the tip-speed ratio. However, here the aim is not to track the actual blade pitch angle, nor local turbulent fluctuations in the wind speed. Indeed, it is the effect of these that should be rejected by the controller. Then, the cluster speed μ_V is considered for the wind speed, and for the blade pitch, a nominal value $\hat{\beta}$ is considered rather than the actual β. This nominal value $\hat{\beta}$ is obtained by solving the power coefficient $C_P(\lambda, \beta)$ table for the nominal power $\lambda_1\hat{P}_{\text{PCC}}$. Then, to get the target thrust, $\hat{\beta}$ is used in the C_T table, that is $C_T(R\overline{\Omega}/\mu_V, \hat{\beta})$ in this case.

3.1.3. Anti-windup strategy   When a turbine reaches the maximum power allowed by the local wind conditions, it will not be able to reach the commanded power set-point, and thus, the integral action of the controller must be temporarily stopped. The anti-windup strategy adopted here is represented by the starred block in Fig. 4, and illustrated in Fig. 5. This represents a "soft" anti-windup algorithm with a smoothed transition between zero and full saturation.

3.2. Discussion

As illustrated in Fig. 4, both the thrust-tracking and power-tracking controls act through the same power command. In typical PI control designs, the effectiveness of each control loop is

ensured by separating them in frequency. For example, an active tower damping controller may act in parallel with the rotor speed controller, since filters are applied to isolate the action of the former to the vicinity of the tower resonant frequency, and remove this frequency from the latter. This frequency separation is not possible here: the specifications call for a controller that can adjust the power so as to track two targets, i.e. rotor thrust and plant power, at once, in the same frequency band. For an individual turbine, this would be impossible. However, since the plant power is the sum of N turbines, it is expected that some of the turbines will be in a position to compensate for imperfect tracking by other turbines.

Note that the controllers can duel, but after some time the power-tracking function will inevitably win. The thought behind the "duelling-controllers" architecture can be stated like this: When the rotor thrust and plant power targets agree, then they reinforce each other, and the turbine will move towards the common set-point quickly. When the rotor thrust and plant power targets disagree, then they partially cancel each other, and the turbine will move towards the power set-point slowly at first, but then more quickly as the thrust error reaches its equilibrium. Therefore, turbines for whom a given power correction is favorable will end up taking more, and those for whom the power correction is unfavorable will take less.

4. Case study
This section presents numerical simulation studies to illustrate the performance of the plant controller. The simulations were carried out using STAS, a unified state-space model of a WPP [18], and the controller is linked to the TotalControl Reference Wind Power Plant (TC-RWP) [15].

4.1. TotalControl Reference Wind Power Plant
The TotalControl Reference Wind Power Plant is a generic wind power plant designed as part of the European H2020 TotalControl project to provide a benchmark for studies on wind power plant control [15]. It consists of 32 turbines of the type DTU 10 MW [19] arranged in four vertical rows in a staggered pattern, as illustrated in Figure 6. The spacing between adjacent turbines in horizontal direction is 5 rotor diameters, in vertical direction 2.5 rotor diameters. The electrical offshore substation has two 66/220 kV transformers rated at 180 MVA each, while the onshore transformer substation has two 220/400 kV transformers. Further specifications are provided in [15, 17, 19].

4.2. Simulation parameters
Each wind turbine model is linearized about an operating point, that is a wind speed of 10 m/s and a power command of 6 MW here. The tuning of the plant controller was conducted on linear transfer-function models, and the parameters are shown in Table 1.

The parameters K_P, K_I, K_T, and ω_T have a crucial influence on the controller behavior and system dynamics, and cannot be set independently as they interact with each other. All the gains were tuned by trial-and-error using a closed-loop dynamic model consisting of the wind turbine, plant controller, and a "grid" that fed the power back with a gain equivalent to the number of turbines in the plant. This represents the worst-case scenario where a disturbance causes all the turbines to respond in unison. Under normal operation, the feedback mechanism through the grid is more diffuse.

A low-pass filter with cut-off frequency of 0.05 Hz is applied to all the inputs, and sets the upper bound on the bandwidth of the controller response. The value of 0.05 Hz is a tradeoff between the speed of the power-tracking response and the rejection of spurious signals, in particular the degree to which high-frequency dynamics adjacent to the tower notch frequency are excited by the feed-through and proportional-gain pathways. The gains K_P and K_I were tuned such that a rapid rise and slight overshoot is observed to a step response, implying a damping
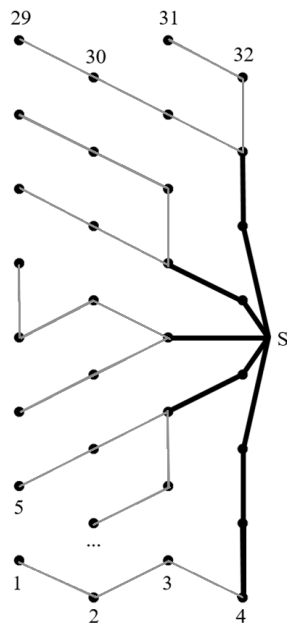
Figure 6. Layout and cable connections of the TotalControl Reference Wind Power Plant [15]. Dots indicate the turbine locations and S indicates the offshore substation.

Variable	Value	Description
K_P	1.0	Proportional gain on power tracking
K_I	$0.4\,\mathrm{s}^{-1}$	Integral gain on power tracking
K_T	$6.0\,\mathrm{m/s}$	Gain on thrust compensation
ω_T	$0.03\,\mathrm{Hz}$	Thust low-pass filter corner frequency

Table 1. Plant controller tuning.

ratio on the control-response mode of around 0.5. The gain K_T and low-pass frequency ω_T were set by scanning the (K_T, ω_T) space, and finding the highest K_T that reduced the thrust over the frequency band $0 \le f < \omega_T$, without introducing undesirable resonance in the power-tracking response. The gains K_P and K_I are such that, when $\lambda N \approx 1$, they dominate K_T.

The simulation results in Section 4.3.2 were obtained using synthetic wind field data averaged over the rotor area, with realistic coherence across the wind plant, following the method of coherence aggregation originally suggested by Sørensen [20, 21]. The data was generated according to empirical spectra representative of offshore sites in the North Sea [22, 23]. These spectra have higher energy content at very low frequencies, exhibiting more variable weather than in standard wind spectra commonly used to design wind turbines [24]. Disturbed flow due to wakes has not been included in this case study for the sake of simplicity, arguing that the focus is on power fluctuations corresponding to the *Weather* part, largely driven by the ambient turbulent wind and not so affected by wakes. In addition, here we assume the component wear rate $\dot{D}^*$ is known, bypassing the spectral modeling of environmental loads (including the *Turbulence* part) and their propagation through the system.

4.3. Simulation results

4.3.1. Frequency response analysis Figure 7 illustrates how the magnitudes of electric power, rotor thrust, rotor speed, and blade pitch vary as the input wind speed changes, for each frequency. These changes may arise from ambient turbulence, harmonic wake fluctuations and/or turbine motions. Different cases are considered for the plant controller: (a) full power tracking and thrust rejection, (b) power tracking is disabled, and (c) both power tracking and thrust rejection are disabled, i.e. the power command is constant to all turbines. The high-frequency part of the frequency response (above 0.1 Hz) is essentially unaffected by the choice of the plant control tuning due to the low-pass and notch filters on the plant control inputs. The spike in
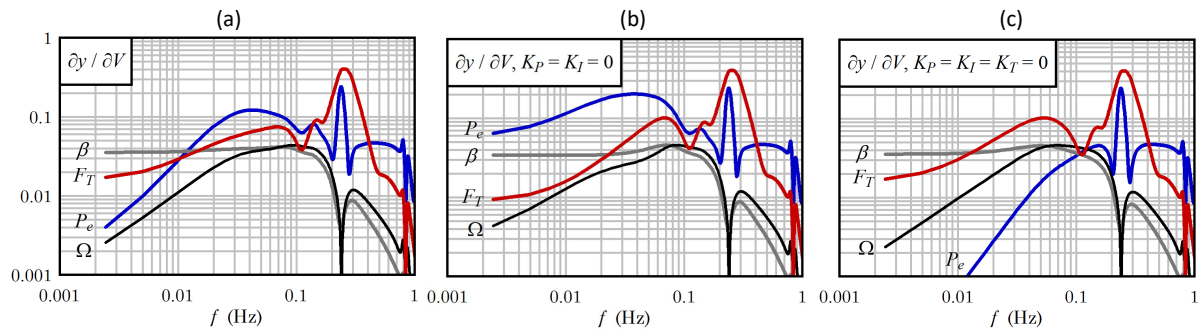
Figure 7. Magnitude of the frequency responses between output electric power P_e (MW), rotor thrust F_T (MN), rotor speed Ω (rad/s), blade pitch β (rad) and input wind speed: (a) full power tracking and thrust rejection; (b) power-tracking is disabled; (c) constant power command.

electrical power at the tower resonant frequency (0.24 Hz) is associated with the active damping of tower side-to-side vibration, which is part of the turbine's internal controller. Thus, for the present purposes, the interesting portion of the curves is below 0.1 Hz.

It can be seen that the power-tracking controller is acting against the thrust compensation in Fig. 7.a. Nonetheless, a comparison with the case when the power command is held constant (Fig. 7.c) indicates that there is a reduction in thrust over a narrow frequency band around 0.03 to 0.08 Hz. The thrust compensation comes at the cost of increased power fluctuations, and the integral effect of the power-tracking controller eventually overwhelms the thrust compensation, such that there is a negligible reduction in thrust below 0.01 Hz. Given the characteristic timescales of atmospheric turbulence, where much of the energy is below 0.01 Hz, it is expected that the default tuning behaves essentially as a power-tracking controller, without much thrust mitigation. However, the situation changes if the power-tracking gains are reduced. Figure 7.b shows the extreme case where power tracking is disabled. In this case, the thrust compensation is effective at low frequencies.

4.3.2. Plant controller performance Here, the turbines are initialized with random damage rates $\dot{D}^*$ between 0 and 1, which are held constant throughout the simulation period. The cluster wind speed (black line) used as an input to the plant controller is shown in Figure 8. The cluster wind speed is calculated from the individual wind turbine speeds as the maximum likelihood computed by a simplified Bayesian method, as explained in [8].

Figure 9 shows the power at the PCC during this scenario, where the power set-point is 192 MW. The set-point per turbine is 6 MW on average, with individual corrections according to the power tracking and thrust compensation pathways. Figure 10 shows the mean and standard deviation of each turbine's rotor thrust and electric power plotted against the damage rate. The result for the case without plant control, i.e. uniform power set-point of 6 MW is also shown in the background. A significant synergy effect by coordinating the operation of wind turbines in a plant is observed. Turbines with low levels of turbulent loading take additional responsibility for power tracking (black dots at the top in the left plot). In the meantime, turbines experiencing high levels of turbulent loading reject part of the low-frequency thrust fluctuations (black dots at the bottom in the left plot). Thus, the severity in rotor thrust fluctuations can be reduced for over half the turbines. Only a few turbines that can best tolerate it, experience an increase in the severity of thrust loading.
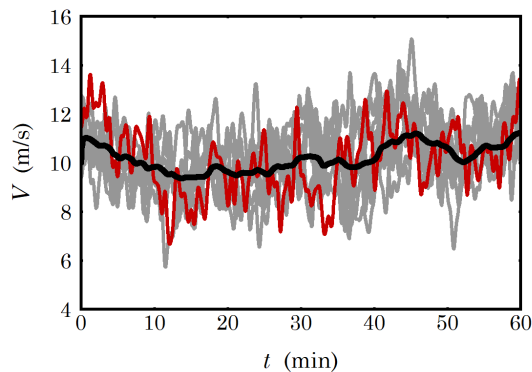
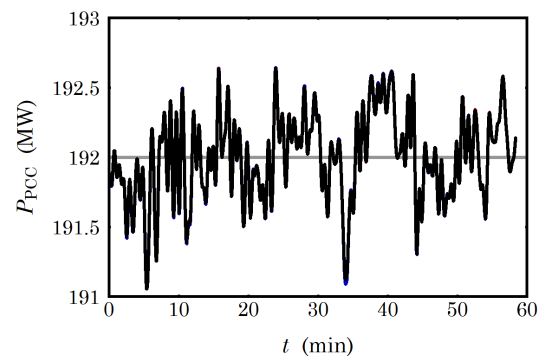**Figure 8.** The cluster wind speed (in black) drawn from individual turbine wind speed estimates.

Figure 9. The power at the PCC (in black) when the set-point is 192 MW.
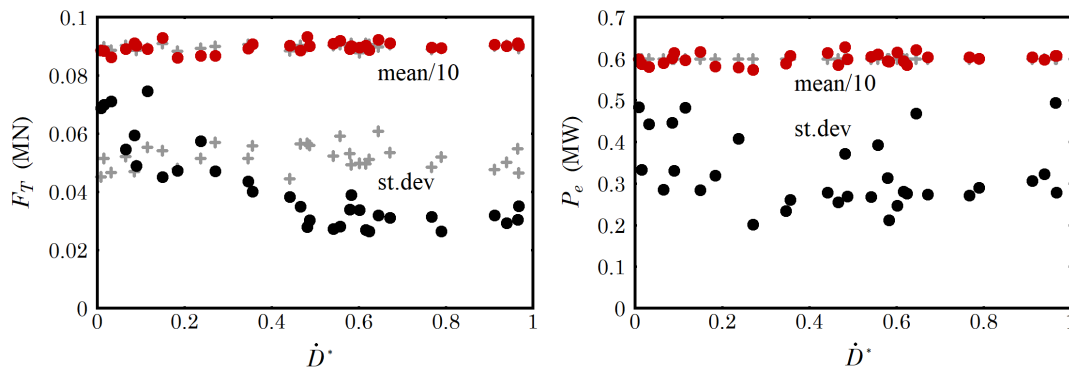

Figure 10. Trends in the mean (red dots) and standard deviation (black dots) of thrust and power fluctuations, as a function of damage rate. Nominal results for the case with a uniform power command are shown in the background.

5. Conclusions

A supervisory control algorithm for large wind power plants has been designed to track a total power command specified by the plant operator, while compensating for fluctuations in rotor thrust at individual wind turbines. The control architecture is based on PI-type algorithms with a filter cascade and look-up tables.

The controller is simple and accessible, and then, it can be useful as a baseline for comparison against more advanced algorithms. However, this simplicity is attained because the controller acts on physically-meaningful inputs, which are not available directly from the raw sensor data. For practical application studies, a state observer should be designed to estimate the severity of loading or fatigue damage. One possible solution for such a state observer is described in [8].

The control performance was verified on a model of the TotalControl Reference Wind Power Plant. Simulation results indicate that the control has the potential to provide a significant reduction in the fluctuating thrust loads experienced by operating wind turbines. On balance, the load reductions on highly-stressed turbines far outweigh the load increases on low-stressed turbines. Thus, there is a definite synergy effect in coordinating the operation of wind turbines across a large wind power plant. Future work includes demonstrating the performance of the algorithm on high-fidelity simulations.

Acknowledgments

References

[1] Hansen A D, Sørensen P, Iov F and Blaabjerg F 2006 Centralised power control of wind farm with doubly fed induction generators *Renewable Energy* **31** 935–951

[2] Soleimanzadeh M, Wisniewski R and Kanev S 2012 An optimization framework for load and power distribution in wind farms *Journal of Wind Engineering and Industrial Aerodynamics* **107-108** 256–262

[3] Riverso S, Mancini S, Sarzo F and Ferrari-Trecate G 2017 Model predictive controllers for reduction of mechanical fatigue in wind farms *IEEE Transactions on Control Systems Technology* **25** 535–549

[4] Kazda J, Merz K, Tande J O and Cutululis N A 2018 Mitigating turbine mechanical loads using engineering model predictive wind farm controller *Journal of Physics: Conference Series* **1104** 012036

[5] Kazda J and Cutululis N A 2020 Model-optimized dispatch for closed-loop power control of waked wind farms *IEEE Transactions on Control Systems Technology* **28** 2029–2036

[6] Madjidian D 2016 Scalable minimum fatigue control of dispatchable wind farms *Wind Energy* **19** 1933–1944

[7] Spudić V, Jelavić M and Baotić M 2011 Wind turbine power references in coordinated control of wind farms *Automatika* **52** 82–94

[8] Merz K, Kölle K, Garcia-Rosa P B and Chabaud V 2020 A hierarchical wind power plant supervisory controller. Report 2020:01124 Tech. rep. SINTEF Energy Research

[9] Bossanyi E and Jorge T 2016 Optimisation of wind plant sector management for energy and loads *2016 European Control Conference (ECC)* pp 922–927

[10] Bossanyi E 2018 Combining induction control and wake steering for wind farm energy and fatigue loads optimisation *Journal of Physics: Conference Series* **1037** 032011

[11] Zhang B, Soltani M, Hu W, Hou P, Huang Q and Chen Z 2018 Optimized power dispatch in wind farms for power maximizing considering fatigue loads *IEEE Transactions on Sustainable Energy* **9** 862–871 ISSN 1949-3037

[12] Mendez Reyes H, Kanev S, Doekemeijer B and van Wingerden J W 2019 Validation of a lookup-table approach to modeling turbine fatigue loads in wind farms under active wake control *Wind Energy Science* **4** 549–561

[13] Pérez-Campuzano D, Gómez de las Heras-Carbonell E, Gallego-Castillo C and Cuerva A 2018 Modelling damage equivalent loads in wind turbines from general operational signals: Exploration of relevant input selection methods using aeroelastic simulations *Wind Energy* **21** 441–459

[14] Dimitrov N 2019 Surrogate models for parameterized representation of wake-induced loads in wind farms *Wind Energy* **22** 1371–1389

[15] Andersen S J, Madariaga A, Merz K, Meyers J, Munters W and Rodriguez C 2018 Reference wind power plant D1.03 Tech. rep.

[16] Merz K and Pedersen M D 2018 *Offshore Wind Turbine Controls* (John Wiley & Sons, Ltd) chap 5, pp 143–237

[17] Merz K, Kölle K and Holdyk A 2018 An electromechanical model of the totalcontrol reference wind power plant. Report 2019:00342 Tech. rep. SINTEF Energy Research

[18] STAS-WPP `https://github.com/SINTEF-Energy-Wind/STAS-WPP` Accessed: 09-03-2021

[19] Bak C, Zahle F, Bitsche R *et al* 2013 Description of the DTU 10 MW reference wind turbine Tech. rep. DTU Wind Energy Report-I-0092, Technical University of Denmark

[20] Sørensen P, Hansen A D and Rosas P A C 2002 Wind models for simulation of power fluctuations from wind farms *Journal of Wind Engineering and Industrial Aerodynamics* **90** 1381–1402 fifth Asia-Pacific Conference on Wind Engineering

[21] Sørensen P, Cutululis N A, Vigueras-Rodríguez A, Madsen H, Pinson P, Jensen L E, Hjerrild J and Donovan M 2008 Modelling of power fluctuations from large offshore wind farms *Wind Energy* **11** 29–43

[22] Vigueras-Rodríguez A, Sørensen P, Cutululis N A, Viedma A and Donovan M H 2010 Wind model for low frequency power fluctuations in offshore wind farms *Wind Energy* **13** 471–482

[23] Vigueras-Rodríguez A, Sørensen P, Viedma A, Donovan M and Gómez Lázaro E 2012 Spectral coherence model for power fluctuations in a wind farm *Journal of Wind Engineering and Industrial Aerodynamics* **102** 14–21

[24] Burton T, Sharpe D, Jenkins N and Bossanyi E 2001 *Wind Energy Handbook* (John Wiley & Sons, Ltd)